

Self-calibrating Quantum State Tomography

Agata M. Brańczyk,¹ Dylan H. Mahler,¹ Lee A. Rozema,¹ Ardavan Darabi,¹ Aephraim M. Steinberg,¹ and Daniel F. V. James¹

¹*CQIQC and IOS, Department of Physics, University of Toronto,
60 Saint George St., Toronto, Ontario M5S 1A7, Canada*

(Dated: September 4, 2022)

We introduce and experimentally demonstrate a technique for performing quantum state tomography on multiple-qubit states using *unknown* unitary operations to perform measurements in different bases. Using our method, it is possible to reconstruct the density matrix of the state up to local $\hat{\sigma}_z$ rotations as well as recover the magnitude of the unknown rotation angle. We demonstrate high-fidelity *self-calibrating tomography* on polarization-encoded one- and two-photon states. The unknown unitary operations are realized in two ways: using a birefringent polymer sheet—an inexpensive smartphone screen protector—or alternatively a liquid crystal wave plate with a tuneable retardance.

Quantum state characterization is essential to the development of quantum technologies, such as quantum computing [1, 2], quantum information [3] and quantum cryptography [4]. The successive measurement of multiple copies of the quantum state and subsequent reconstruction of the state's density matrix is known as *quantum state tomography* (QST) [5, 6].

Standard QST can not be implemented in systems which preclude access to known unitary transformations, such as photosynthetic systems [7, 8] where the transition dipole moment is not known with high accuracy. With such systems in mind we introduce a method for *self-calibrating tomography* (SCT), which successfully reconstructs the state of the system using *unknown* unitary operations. Quantum process tomography of photosynthetic systems using ultrafast spectroscopy was proposed by Yuen-Zhou *et al.* [9, 10].

Our method for self-calibrating tomography may also improve the robustness of standard tomography, where calibrated unitary operations undergo small errors and fluctuations over the course of the experiment. For other modifications to standard QST due to inaccessible information or preferable measurements choices, we refer the reader to references [11–14].

We find that given local unitary operations with unknown rotation angles, and known and adjustable rotation axes, it is possible to reconstruct the density matrix of a state up to local $\hat{\sigma}_z$ rotations, as well as recover the magnitude of the unknown rotation angles.

We demonstrate SCT in a linear-optical system, using polarized photons as qubits. An inexpensive smartphone screen protector, i.e. an uncharacterized birefringent polymer sheet, is used to change the measurement basis.

We go on to investigate the technique's robustness to measurement noise and retardance magnitude, and demonstrate SCT of a two-qubit state using liquid crystal wave plates with tuneable retardances.

The state of a qubit, given by the density matrix $\hat{\rho}$,

can be decomposed into a sum of orthogonal operators

$$\hat{\rho} = \frac{1}{2} \sum_{i=0}^3 \lambda_i \hat{\sigma}_i, \quad (1)$$

where $\hat{\sigma}_0$ is the identity operator and $\hat{\sigma}_{1-3}$ are the Pauli matrices. The coefficients λ_j are given by the expectation values of the basis operators, $\lambda_i = \text{Tr}[\hat{\rho} \hat{\sigma}_i]$.

Projective measurements of subsequent copies of the state lead to measurement statistics given by expectation values $n_j = \mathcal{N}_j \text{Tr}[\hat{\rho} \hat{\mu}_j(\alpha)]$ where α characterizes the projector $\hat{\mu}_j(\alpha) = \hat{U}_j(\alpha)^\dagger \hat{\mu}_0 \hat{U}_j(\alpha)$ with respect to a trusted, fixed projector $\hat{\mu}_0$. \mathcal{N}_j is a constant that depends on the duration of data collection, detector efficiency, loss etc. The relationship between the measurement statistics and the parameters which characterize the density matrix is given by

$$n_j = \frac{\mathcal{N}_j}{2} \sum_{i=0}^3 \text{Tr}[\hat{\mu}_j(\alpha) \hat{\sigma}_i] \lambda_i. \quad (2)$$

If \mathcal{N}_j is unknown, but $\mathcal{N}_k = \mathcal{N}_l \forall k, l$, it can be determined from the normalization condition $\lambda_0 = 1$. In standard tomography, α is a known parameter and it is sufficient to measure only four different expectation values n_j to solve Eq. (2) for λ_i (only three n_j are required if \mathcal{N}_j is known). Given an *uncalibrated* unitary operation, i.e. an unknown α , an additional measurement is required to solve for both λ_i and α .

Measurements are chosen such that $\hat{\mu}_j(\alpha)$ generate a set of five linearly independent equations from Eq. (2). If this condition is met, the equations yield two sets of solutions, corresponding to $\pm \alpha$, i.e. either the actual state or the phase-flipped version of the state.

It is straightforward, but non-trivial, to extend this formalism to multiple-qubit systems. However this is not required as in practice one may use a maximum likelihood estimation method [5, 15] adapted for SCT to reconstruct the density matrix [16].

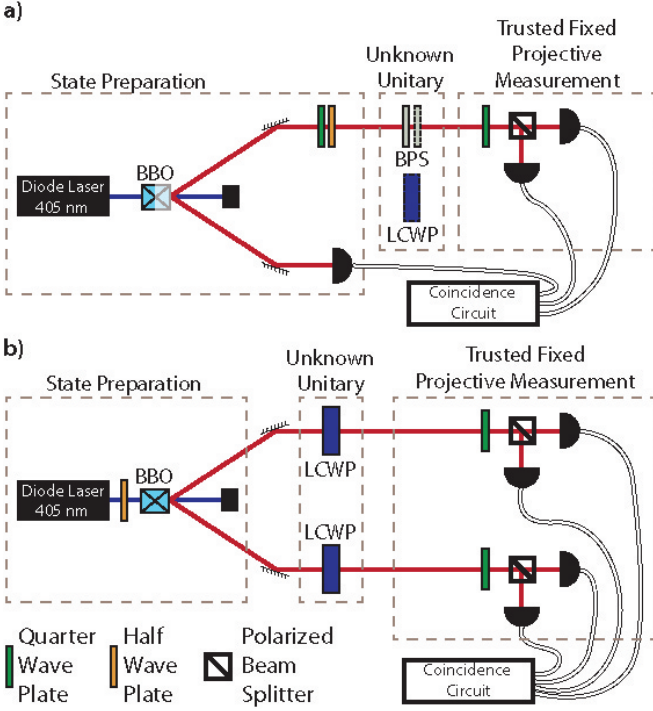


FIG. 1: Experimental scheme: a) A single-qubit state is prepared, unknown unitary operations are implemented using BPSs or an LCWP and the state is measured using a trusted, fixed measurement; b) An entangled two-qubit state is prepared, unknown local unitary operations are implemented using LCWPs and the two-qubit state is measured using a trusted, fixed measurement.

For a linear-optical test of this method, we performed SCT on polarization-encoded one- and two-qubit states. Single-qubit states were prepared by pumping a 1mm long type-I down-conversion beta-barium borate (BBO) crystal with a 405nm diode laser, as shown in Fig. 1 a). The detection of a horizontally polarized photon in one spatial mode of the down-converted photon-pair heralds the presence of a horizontally polarized photon in the other mode. Quarter- and half-wave plates then prepare arbitrary polarization states. For the trusted, fixed projector, we chose $\hat{\mu}_0 = |R\rangle\langle R|$, implemented with a quarter-wave plate and a polarizing beamsplitter, followed by coincidence-counting. We constructed additional operators $\hat{\mu}_j(\alpha) = \hat{U}_j(\alpha)^\dagger \hat{\mu}_0 \hat{U}_j(\alpha)$ using different implementations of $\hat{U}_j(\alpha)$: $\hat{U}_1(\alpha) = R_x(\alpha)$; $\hat{U}_2(\alpha) = R_y(\alpha)$; $\hat{U}_3(\alpha) = R_x(-2\alpha)$; $\hat{U}_4(\alpha) = R_y(-2\alpha)$, where $R_\nu(\alpha) = \cos(\frac{\alpha}{2})\hat{\sigma}_0 - i\sin(\frac{\alpha}{2})\hat{\sigma}_\nu$ are rotations about the ν axis by angle α and $\hat{\sigma}_i$ are in the R/L basis. Note that rotations of 2α were required to satisfy the linear-independence condition on Eq. (2). These rotations were realized with a double-pass through a birefringent polymer sheet (BPS)—the sheet was cut in half and the pieces placed in succession. The beam passed through sections

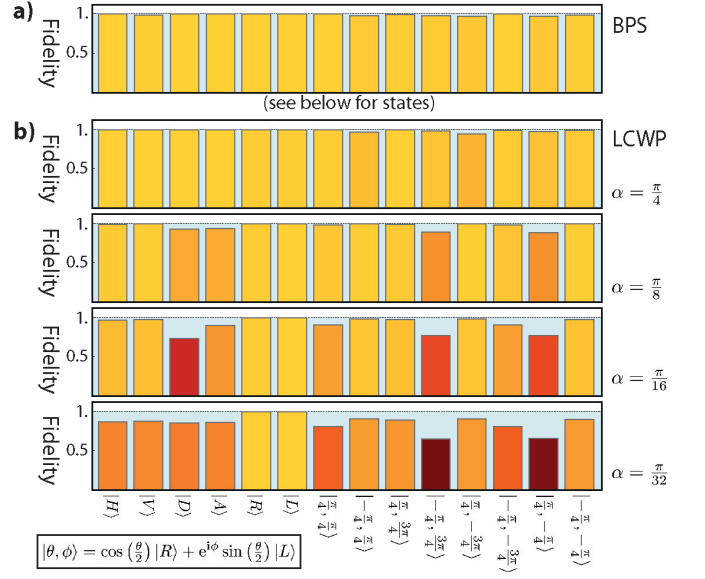


FIG. 2: Single-shot fidelity between SCT and ST for 14 states distributed on the Bloch sphere, using: a) a birefringent polymer sheet (BPS) as the uncalibrated wave plate; and b) using a liquid crystal wave plate (LCWP) set to different values of the retardance α .

of the pieces that were within close proximity before partition, to ensure consistency in the birefringence. One piece was then removed to perform rotations of α , before removal of the remaining piece to measure $\hat{\mu}_0$. This measurement sequence eliminated the need for realignment between measurements. Alignment of the fast axis with respect to the state prescribed the rotation axis of the unitary. Both output ports of the PBS were measured to determine \mathcal{N}_j .

Using this method, SCT was performed on 14 states: six that lie at the ends of the three axes and eight other states defined by all combinations of $\theta = \pm\frac{\pi}{4}$ and $\phi = \{\pm\frac{\pi}{4}, \pm\frac{3\pi}{4}\}$ where $|\psi\rangle = \cos(\frac{\theta}{2})|R\rangle + e^{i\phi}\sin(\frac{\theta}{2})|L\rangle$. Each state was reconstructed using a maximum-likelihood estimation method. For comparison, standard tomography (ST) was also performed on each of the states. We used the fidelity $F = \text{Tr}[\sqrt{\hat{\rho}_{\text{ST}}\hat{\rho}_{\text{SCT}}}\sqrt{\hat{\rho}_{\text{ST}}}]^2$ to characterize the success of SCT, where $\hat{\rho}_{\text{ST}}$ and $\hat{\rho}_{\text{SCT}}$ are the density operators given by ST and SCT respectively. We achieved an average fidelity $\bar{F} = 0.99 \pm 0.01$ and determined the retardance of the BPS (at 405nm) to be $\alpha = 0.58 \pm 0.03$ (close to $\pi/6$). Individual fidelities for each state are shown in Fig. 2 a).

To determine the effectiveness of SCT as a function of the retardance, we repeated the experiment using Bold-erVision Optik liquid crystal wave plates (LCWP). In an LCWP, the birefringence is a function of the applied voltage, allowing for the retardance to be set arbitrarily. A single LCWP was used to implement rotations of α and 2α using different voltage settings. Fidelities for different

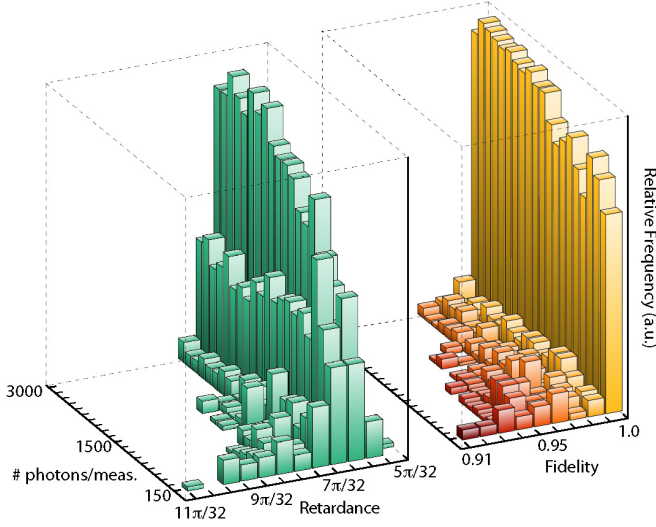


FIG. 3: A histogram showing the predicted retardance and the fidelity between SCT and ST, for 100 runs of SCT with varying numbers of total photons collected (and hence levels of counting error). All used $|\psi\rangle = |H\rangle$ and the BPS.

setting of α are shown in Fig. 2 b). The average fidelity decreases with the size of the retardance. The fidelity for states $|\psi\rangle = |R\rangle$ and $|\psi\rangle = |L\rangle$ always remains close to unity. This is a consequence of our choice of measurement projectors. Using the LCWP, we find a slightly lower average fidelity with a greater spread over the different states, even for values of α larger than that of the BPS. We attribute this to errors associated with the non-linear dependence of the retardance on the voltage passed through the LCWP. This influences how accurately 2α can be set with respect to α .

To investigate the dependence of the fidelity on the amount of noise, we performed SCT on the state $|\psi\rangle = |H\rangle$ using a retardance $\alpha = \pi/32$. The noise scales inversely with the square root of the number of counts and by collecting from 150 to 3000 photons we varied the noise between roughly 1% and 10%. For each noise setting, tomography was repeated 100 times. The resulting fidelities and predicted retardances are presented in Fig. 3. Notice a smaller second peak in the high-noise region at $F \approx 0.95$ and $\alpha \approx 9\pi/32$. The maximum likelihood algorithm sometimes converges to a state and retardance that do not correspond to the actual state. We note that given prior knowledge of the purity of the state, it is possible to modify the algorithm to exclude the false maxima [16]. As the noise decreases, only high-fidelity results corresponding to the actual retardance remain. Fig. 4 shows the distribution of states on the Bloch sphere as predicted by SCT for high and low noise amounts.

For multi-qubit tomography, entangled two-qubit states, $|\psi\rangle = a|HH\rangle + b|VV\rangle$, were prepared using two 1mm long type-I down-conversion BBO crystals with op-

C_{SCT}	C_{ST}	F
0.905 ± 0.005	0.927 ± 0.003	0.968 ± 0.0028 *
0.566 ± 0.005	0.562 ± 0.005	0.978 ± 0.0012
0.337 ± 0.005	0.328 ± 0.004	0.977 ± 0.0032
0.004 ± 0.004	0.010 ± 0.003	0.989 ± 0.0015 **

TABLE I: The concurrence $C = 2ab$ as predicted by both tomographic techniques and fidelity between the two reconstructions for states with different degrees of entanglement. Density matrices for * and ** are shown in Figure 5 a) and b) respectively. Error bars were determined by using Poissonian noise in a Monte Carlo simulation

tical axes aligned in perpendicular planes [17] pumped by a 405nm, diode laser, as shown in Fig. 1 b). The parameters a and b were tuned by changing the polarization of the pump beam with a HWP. LCWPs in each arm, implemented the unknown unitary operations, followed by detection of $\hat{\mu}_0 = |R\rangle\langle R|$ in both modes. For this two-qubit experiment, LCWPs were chosen over the BPSs due to realignment issues that accompany the insertion (as opposed to removal) of optical elements in the beam-path. Fidelities between SCT and ST are shown for a variety of entangled states in Table I.

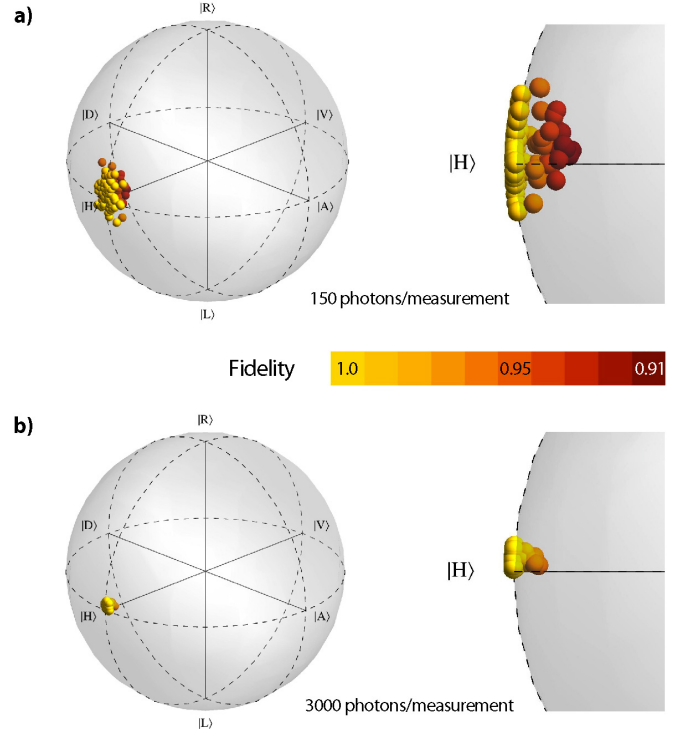


FIG. 4: Distribution of states on the Bloch sphere as predicted by SCT for: a) high noise; and b) low noise. Notice the somewhat separate clump of lower-fidelity states in a). There are 100 states shown in each sphere.

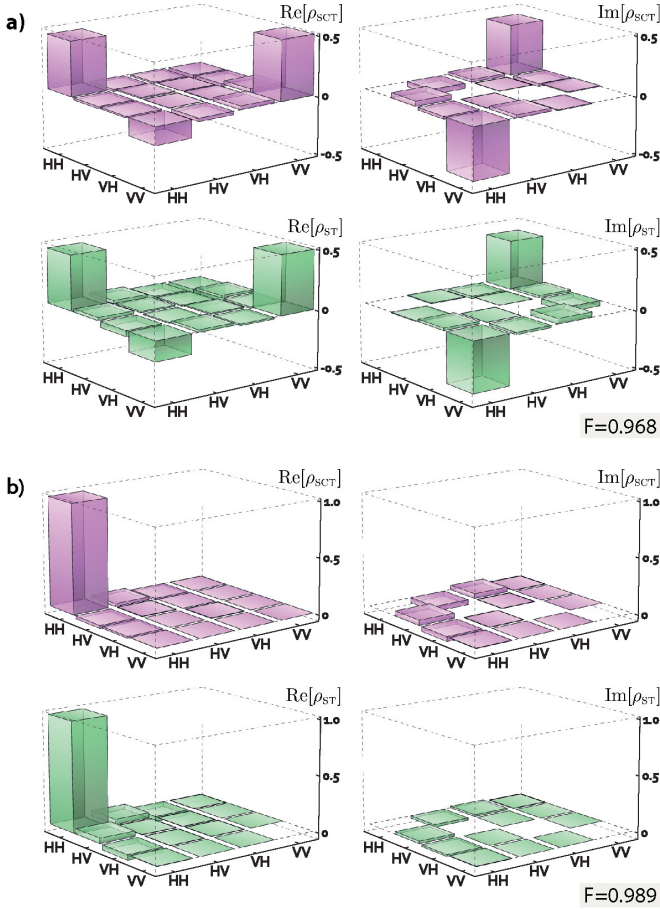


FIG. 5: Comparison between density matrices reconstructed using SCT and ST: a) $F = 0.968 \pm 0.0028$; b) $F = 0.989 \pm 0.0015$. For concurrences and other fidelities, refer to Table I.

Fig 5 shows density matrices for the most- and least-entangled states. The retardances were determined to be $\alpha_1 = 0.810 \pm 0.009$ and $\alpha_2 = 0.760 \pm 0.006$, compared with the known value $\alpha = \pi/4 \approx 0.785$.

In conclusion, we have introduced and demonstrated a technique for performing quantum state tomography of multi-qubit systems which does not rely on complete knowledge of the unitary operation used to change the measurement basis. Our technique characterizes the state of interest with high fidelity as well as recovering the unknown unitary operation. Remarkably, we find that in the context of QST of polarization-encoded qubits, it is possible to do away with a well-calibrated half-wave plate and replace it with an inexpensive uncharacterized piece of birefringent material.

A future extension of this work will attempt to incorporate unknown rotation axes and non-unitary transformations, such as those that introduce noise to the system, thereby reducing the purity of the state by an unknown amount.

We anticipate our method to be applicable to quan-

tum state tomography of multi-chromophore systems in photosynthesis, where the unknown unitary operations can be implemented using laser pulses. The angle of rotation is proportional to the square root of the intensity, allowing for rotations of α and 2α even if α is unknown, and the phase of the pulse will determine the rotation axis. The trusted, fixed measurement will measure the intensity of the emitted light, which is proportional to the expectation value of the excited state of the chromophores.

AMB, AD and DFVJ thank DARPA (QuBE) for support. DHM, LAR and AMS thank NSERC, CIFAR and QuantumWorks for support. We also thank Xingxing Xing for the serendipitous discovery of the birefringence of his smartphone screen protector.

-
- [1] P. Kok, W. J. Munro, K. Nemoto, T. C. Ralph, J. P. Dowling, and G. J. Milburn, *Rev. Mod. Phys.* **79**, 135 (pages 40) (2007), URL <http://link.aps.org/abstract/RMP/v79/p135>.
 - [2] A. M. Childs and W. van Dam, *Rev. Mod. Phys.* **82**, 1 (2010), URL <http://link.aps.org/doi/10.1103/RevModPhys.82.1>.
 - [3] M. A. Nielsen and I. L. Chuang, *Quantum computation and quantum information* (Cambridge University Press, Cambridge, 2000).
 - [4] C. H. Bennett and G. Brassard, in *Proceedings of IEEE International Conference on Computers, Systems and Signal Processing* (IEEE, New York, 1984), pp. 175–179, bangalore, India, December 1984.
 - [5] D. F. V. James, P. G. Kwiat, W. J. Munro, and A. G. White, *Phys. Rev. A* **64**, 052312 (2001), URL <http://link.aps.org/doi/10.1103/PhysRevA.64.052312>.
 - [6] J. B. Altepeter, D. F. V. James, and P. G. Kwiat, *Qubit Quantum State Tomography* (Springer, 2004), chap. 4.
 - [7] G. S. Engel, T. R. Calhoun, E. L. Read, T.-K. Ahn, T. Mancal, Y.-C. Cheng, R. E. Blankenship, and G. R. Fleming, *Nature* **446**, 782 (2007), URL <http://dx.doi.org/10.1038/nature05678>.
 - [8] E. Collini, C. Y. Wong, K. E. Wilk, P. M. G. Curmi, P. Brumer, and G. D. Scholes, *Nature* **463**, 644 (2010), URL <http://dx.doi.org/10.1038/nature08811>.
 - [9] J. Yuen-Zhou and A. Aspuru-Guzik, **134**, 134505 (2011), ISSN 00219606, URL <http://dx.doi.org/doi/10.1063/1.3569694>.
 - [10] J. Yuen-Zhou, J. J. Krich, M. Mohseni, and A. Aspuru-Guzik, *Proceedings of the National Academy of Sciences* **108**, 17615 (2011), <http://www.pnas.org/content/108/43/17615.full.pdf+html>, URL <http://www.pnas.org/content/108/43/17615.abstract>.
 - [11] R. B. A. Adamson, L. K. Shalm, M. W. Mitchell, and A. M. Steinberg, *Phys. Rev. Lett.* **98**, 043601 (2007), URL <http://link.aps.org/doi/10.1103/PhysRevLett.98.043601>.
 - [12] R. B. A. Adamson, P. S. Turner, M. W. Mitchell, and A. M. Steinberg, *Phys. Rev. A* **78**, 033832 (2008), URL <http://link.aps.org/doi/10.1103/PhysRevA.78.033832>.

- 78.033832.
- [13] R. B. A. Adamson and A. M. Steinberg, Phys. Rev. Lett. **105**, 030406 (2010), URL <http://link.aps.org/doi/10.1103/PhysRevLett.105.030406>.
 - [14] Z. E. D. Medendorp, F. A. Torres-Ruiz, L. K. Shalm, G. N. M. Tabia, C. A. Fuchs, and A. M. Steinberg, Phys. Rev. A **83**, 051801 (2011), URL <http://link.aps.org/doi/10.1103/PhysRevA.83.051801>.
 - [15] J. Lofberg, in *Computer Aided Control Systems Design*, 2004 IEEE International Symposium on (2004), pp. 284–289.
 - [16] A. M. Brańczyk and D. F. V. James, in preparation.
 - [17] P. G. Kwiat, E. Waks, A. G. White, I. Appelbaum, and P. H. Eberhard, Phys. Rev. A **60**, R773 (1999), URL <http://link.aps.org/doi/10.1103/PhysRevA.60.R773>.